pharmaceuticals

MDPI

Article

Synthesis and Structure Determination of Substituted Thiazole Derivatives as EGFR/BRAF^{V600E} Dual Inhibitors Endowed with Antiproliferative Activity

Lamya H. Al-Wahaibi [1,*], Essmat M. El-Sheref [2], Alaa A. Hassan [2], S. Bräse [3,*], M. Nieger [4], Bahaa G. M. Youssif [5,*], Mahmoud A. A. Ibrahim [2,6] and Hendawy N. Tawfeek [2,7]

1 Department of Chemistry, College of Sciences, Princess Nourah Bint Abdulrahman University, Riyadh 11564, Saudi Arabia
2 Chemistry Department, Faculty of Science, Minia University, El Minia 61519, Egypt; essmat_elsheref@mu.edu.eg (E.M.E.-S.); alaahassan2001@mu.edu.eg (A.A.H.); m.ibrahim@compchem.net (M.A.A.I.); hendawy1976@yahoo.com (H.N.T.)
3 Institute of Biological and Chemical Systems, IBCS-FMS, Karlsruhe Institute of Technology, 76131 Karlsruhe, Germany
4 Department of Chemistry, University of Helsinki, P.O. Box 55 (A. I. Virtasen aukio 1), 00014 Helsinki, Finland; martin.nieger@helsinki.fi
5 Pharmaceutical Organic Chemistry Department, Faculty of Pharmacy, Assiut University, Assiut 71526, Egypt
6 School of Health Sciences, University of KwaZulu-Natal, Westville Campus, Durban 4000, South Africa
7 Unit of Occupational of Safety and Health, Administration Office of Minia University, El-Minia 61519, Egypt
* Correspondence: lhalwahaibi@pnu.edu.sa (L.H.A.-W.); stefan.braese@kit.edu (S.B.); bgyoussif2@gmail.com (B.G.M.Y.)

Abstract: 2,3,4-trisubstituted thiazoles **3a–i**, having a methyl group in position four, were synthesized by the reaction of 1,4-disubstituted thiosemicarbazides with chloroacetone in ethyl acetate/Et_3N at room temperature or in ethanol under reflux. The structures of new compounds were determined using NMR spectroscopy, mass spectrometry, and elemental analyses. Moreover, the structure of compound **3a** was unambiguously confirmed with X-ray analysis. The cell viability assay of **3a–i** at 50 µM was greater than 87%, and none of the tested substances were cytotoxic. Compounds **3a–i** demonstrated good antiproliferative activity, with GI_{50} values ranging from 37 to 86 nM against the four tested human cancer cell lines, compared to the reference erlotinib, which had a GI_{50} value of 33 nM. The most potent derivatives were found to be compounds **3a**, **3c**, **3d**, and **3f**, with GI_{50} values ranging from 37 nM to 54 nM. The EGFR-TK and BRAF^{V600E} inhibitory assays' results matched the antiproliferative assay's results, with the most potent derivatives, as antiproliferative agents, also being the most potent EGFR and BRAF^{V600E} inhibitors. The docking computations were employed to investigate the docking modes and scores of compounds **3a**, **3c**, **3d**, and **3f** toward BRAF^{V600E} and EGFR. Docking computations demonstrated the good affinity of compound **3f** against BRAF^{V600E} and EGFR, with values of −8.7 and −8.5 kcal/mol, respectively.

Keywords: thiazole; thiosemicarbazide; X-ray; viability; antiproliferative; molecular modeling

check for updates

Citation: Al-Wahaibi, L.H.; El-Sheref, E.M.; Hassan, A.A.; Bräse, S.; Nieger, M.; Youssif, B.G.M.; Ibrahim, M.A.A.; Tawfeek, H.N. Synthesis and Structure Determination of Substituted Thiazole Derivatives as EGFR/BRAF^{V600E} Dual Inhibitors Endowed with Antiproliferative Activity. *Pharmaceuticals* **2023**, *16*, 1014. https://doi.org/10.3390/ph16071014

Academic Editor: Valentina Onnis

Received: 17 June 2023
Revised: 12 July 2023
Accepted: 13 July 2023
Published: 17 July 2023

1. Introduction

Kinases control many essential cancer processes, including tumor growth, metastasis, neovascularization, and treatment resistance. Hence, the development of kinase inhibitors has become a top priority, with several of them receiving FDA approval for a variety of cancer purposes [1–5].

One approach for simultaneously inhibiting two or more targets is combination chemotherapy. However, two or more drugs' pharmacokinetic profiles and metabolic stabilities frequently differ. Furthermore, drug–drug interactions may occur during combination chemotherapy [6–8]. An alternative method for addressing these issues is to

use a single drug to suppress two or more targets [9–12]. This approach may even make patients' treatment easier. The FDA has approved many dual-target or multi-target cancer treatments. Dasatinib is a multi-targeted kinase inhibitor that can potentially be a highly effective anticancer medication [13–17].

The acquired $BRAF^{V600E}$ mutation was suggested as a resistance mechanism after therapy with an EGFR inhibitor [18,19]. The development of resistance in colorectal cancer was also linked to the feedback stimulation of EGFR signaling [20–22]. Additionally, BRAF inhibition can cause EGFR to become active, promoting tumor growth [23,24]. A BRAF/EGFR combination was used to adopt these issues. In a number of studies, the BRAF/EGFR combination was found to have a significant therapeutic effect in patients with metastatic colorectal cancer that had $BRAF^{V600E}$ mutations [18,25,26]. As a result, sequentially inhibiting the two kinases may provide a solution to the EGFR activation problem.

Thiazole and its derivatives are also among the most active chemicals, ranking first in anticancer activity [27–29]. As well, thiazole-containing molecules were identified in a number of therapeutically available anticancer medicines (Figure 1), including tiazofurin (**I**) [30], dasatinib (**II**) [31,32], and dabrafenib (**III**) [33,34].

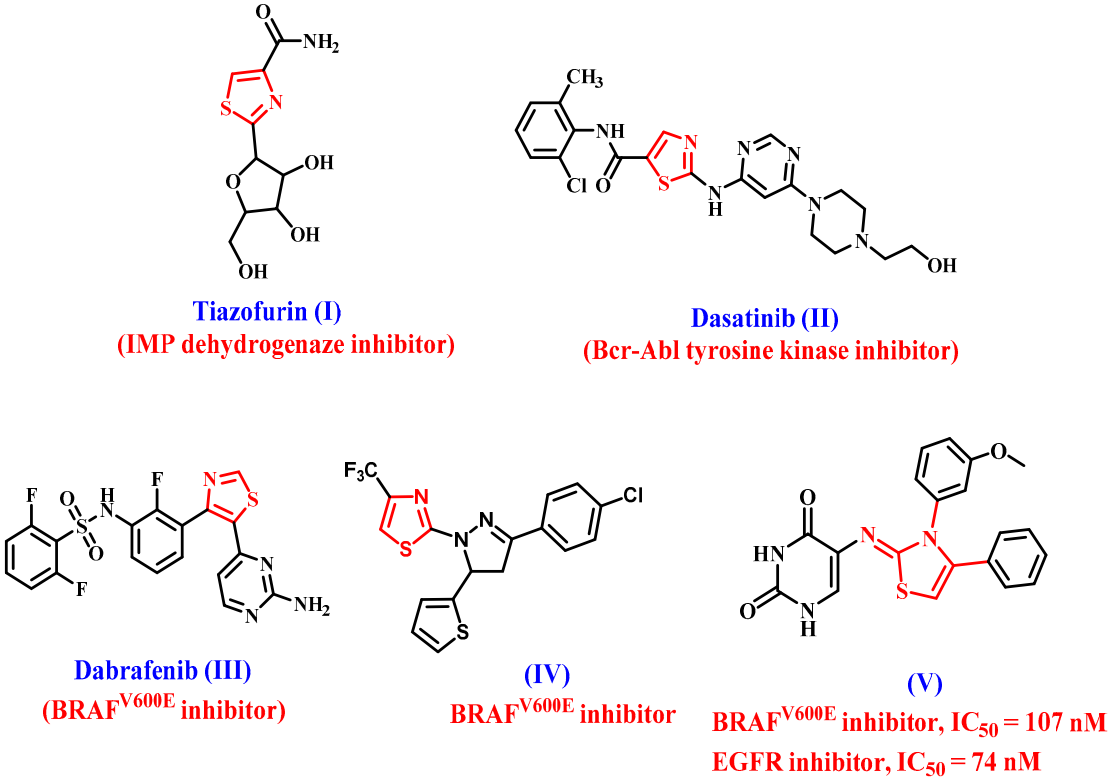

Figure 1. Structures of thiazole-based anticancer drugs **I**–**III** and compounds **IV** and **V**.

Abdel-Maksoud et al. [35] investigated several thiazole-based compounds as potential $BRAF^{V600E}$ inhibitors. Compound **IV** (Figure 1) had the most potent antiproliferative activity, with a competitive $BRAF^{V600E}$ inhibitory action (IC_{50} = 0.05 μM). Furthermore, compound **IV** significantly affected dose-dependent apoptosis.

We recently reported on the design and synthesis of two series of thiazole-based compounds as potent antiproliferative agents targeting EGFR and $BRAF^{V600E}$ [36]. Compound **V** (Figure 1) was shown to be the most potent derivative of all synthesized compounds, with a GI_{50} value of 0.90 μM against the four evaluated cancer cell lines when compared to the reference doxorubicin (GI_{50} = 1.10 μM). Compound **V** inhibited EGFR and $BRAF^{V600E}$ with IC_{50} values of 74 ± 7 and 107 ± 10 nM, respectively, and was more effective than erlotinib against EGFR (IC_{50} = 80 nM).

Moreover, the sulfonamide moiety is commonly employed in medicinal chemistry as efficient bioisosteres of the carboxylic group [37,38]. The sulfonamide motif could build a network of hydrogen bonds similar to the carboxylic group. As the carboxylic group's bioisosteres, it could avoid some of the carboxylic group's limitations, such as metabolic instability, toxicity, and limited passive diffusion across biological membranes [37]. As a result, the sulfonamide moiety gained popularity in medicinal chemistry, and a wide range of sulfonamide derivatives with diverse biological properties, such as anticancer activity [39–41], were produced.

In light of the aforementioned information, and as part of our enduring effort to develop potent antiproliferative agents that are dual inhibitors of EGFR and $BRAF^{V600E}$ [42–45], we describe the synthesis of a new set of thiazole-based compounds **3a–i** (Figure 2) in this article as antiproliferative agents that target EGFR and/or mutant BRAF. Scaffold A and B molecules had a methyl group in position 4, a hydrazo group in position 2, a physiologically active tosyl group for the scaffold B compounds, and a 2,4-dinitrophenyl group for the scaffold A compounds (Figure 2). The cell viability of the novel derivatives was tested against a normal human mammary gland epithelial (MCF-10A) cell line. The antiproliferative action of **3a–i** was tested on a panel of four human cancer cell lines. The ability to inhibit EGFR and mutant BRAF was further assessed for the most active antiproliferative derivatives. Finally, the most potent compounds' binding modes and docking scores toward $BRAF^{V600E}$ and EGFR targets were investigated.

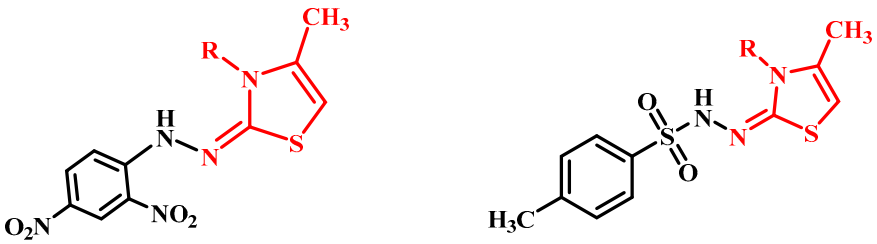

Scaffold A (3a-f)

3a, R = $CH_2C_6H_5$
3b, R = CH_2CH_3
3c, R = $CH_2CH{=}CH_2$
3d, R = C_6H_{11}
3e, R = C_6H_5
3f, R = 4-$CH_3C_6H_6$

Scaffold B (3g-i)

3g, R = C_6H_5
3h, R = $CH_2CH{=}CH_2$
3i, R = CH_2CH_3

Figure 2. The new target compounds' **3a–i** structures.

2. Results and Discussion

2.1. Chemistry

This study aimed to develop new thiazole derivatives in a straightforward manner. Indeed, a novel series of *(Z)*-3-substituted-2-(2-substituted)-hydrazinylidene)-4-methyl-2,3-dihydrothiazoles **3a–i** were synthesized in an excellent yield of 78–99% via a mixture of substituted hydrazine-carbothioamides **1a–i** [46–49] and chloroacetone (**2**) in ethyl acetate as a solvent. Et_3N catalyzed the reaction by stirring overnight at room temperature or refluxing in ethanol for 6–10 hrs (Scheme 1). For example, compound **3a** was obtained in ($AcOEt/Et_3N$: 98%) and (EtOH: 85%) yield after recrystallization (Table 1). The structure assignment for all obtained products **3a–i** was confirmed by IR, NMR analysis (Supplementary File Figures S2–S32) of the expected chemical shifts, mass spectrometry, elemental analysis, and X-ray crystallography.

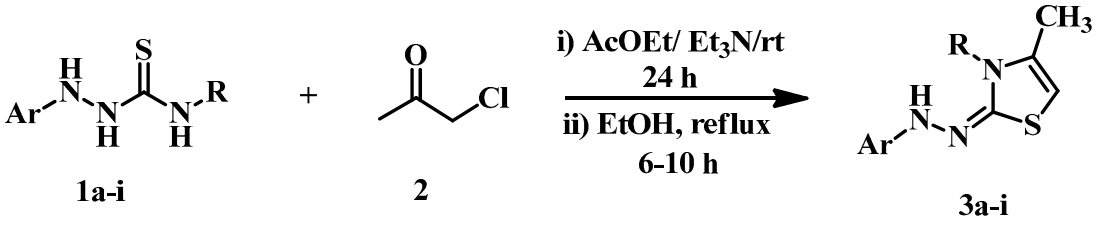

1,3: a, Ar = 2,4-di-NO_2-C_6H_3-, R = -$CH_2C_6H_5$
b, Ar = 2,4-di-NO_2-C_6H_3-, R = -CH_2CH_3
c, Ar = 2,4-di-NO_2-C_6H_3-, R = -$CH_2CH{=}CH_2$
d, Ar = 2,4-di-NO_2-C_6H_3-, R = -C_6H_{11}
e, Ar = 2,4-di-NO_2-C_6H_3-, R = -C_6H_5
f, Ar = 2,4-di-NO_2-C_6H_3-, R = 4-CH_3-C_6H_5-
g, Ar = *p*-CH_3-$C_6H_4SO_2$-, R = -C_6H_5
h, Ar = *p*-CH_3-$C_6H_4SO_2$-, R = -$CH_2CH{=}CH_2$
i, Ar = *p*-CH_3-$C_6H_4SO_2$-, R = -CH_2CH_3

Scheme 1. Syntheses of substituted thiazoles **3a–i**.

Table 1. Yield percentage of **3a–i** via method **A** and method **B**.

Compound	3a	3b	3c	3d	3e	3f	3g	3h	3i
Method A	98	99	96	94	94	92	90	89	87
Method B	85	84	83	78	83	86	83	83	78

Compound **3a** was chosen as a representative example, which was assigned as (*Z*)-3-benzyl-2-(2-(2,4-dinitrophenyl)hydrazinylidene)-4-methyl-2,3-dihydrothiazole and exhibited a molecular formula $C_{17}H_{15}N_5O_4S$ with mass *m/z* (385). Elemental analysis and mass spectrometry confirmed that **3a** was formed by an interaction between one mole of *N*-benzyl-2-(2,4-dinitrophenyl)hydrazinecarbothioamide (**1a**) and one mole of chloroacetone (**2**), with the loss of a molecule of HCl and another molecule of H_2O. FTIR analysis of thiazole compound **3a** showed different peaks at 3286 cm^{-1} due to hydrazo-NH stretching, 3085 cm^{-1} for aromatic stretching-CH, and 2978 cm^{-1} for aliphatic-CH as well as two peaks at 1609 and 1548 cm^{-1} for C=N and C=C, respectively. IR showed a peak at 1399 and 1117 cm^{-1} for the NO_2 group. Further, in the ^{1}H NMR spectrum of **3a**, five singlet signals were distinguished at δ_H = 1.98, 5, 6.42, 8.68, and 10.38 ppm, which were assigned as CH_3, benzyl-CH_2, thiazole-H, 2,4-dinitrophenyl-H-3, and hydrazono-NH, respectively (Figure 3). The ^{13}C NMR spectrum for compound **3a** revealed signals at δ_C = 13.78, 47.16, and 94.49 ppm, which were assigned as CH_3, benzyl-CH_2, and thiazole-C5, respectively. Moreover, C4 and C2 gave signals at δ_C = 135.13 and 164.14 ppm, respectively.

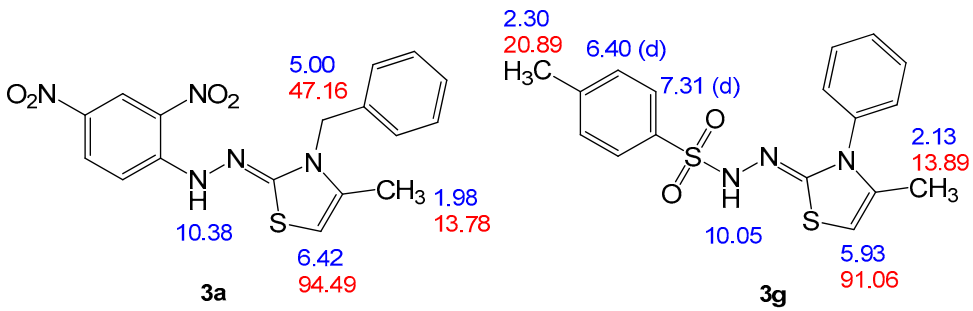

Figure 3. Structure elucidation of compounds **3a** and **3g**.

To make comparable results, we chose another compound, **3g**, which was assigned as (*Z*)-4-methyl-*N*′-(4-methyl-3-phenylthiazol-2(3*H*)-ylidene) benzenesulfonohydrazide, with a molecular formula $C_{17}H_{17}N_3O_2S_2$ (*m/z* = 359). Compound **3g** is analogous for

the above compound by replacing the benzyl group and 2,4-dinitrophenyl with phenyl and 4-methyl-benzensulfonoyl groups, respectively. The ^{1}H NMR for this compound is similar for compound **3a** unless the 1,4-disubstituted benzene gives characteristic signals as a doublet at δ_H = 6.40 (d, 2H) and 7.31 ppm (d, 2H), which were assigned as H-*m* and H-*o*, respectively. Moreover, by comparing the data for the two compounds, as shown in Figure 3, it is clear that the reaction behaves the same with the difference in the substitutes and that the difference is a slight difference in the chemical shift's results for the difference only in the nature of the substituted groups.

Another example is compound **3b,** which was assigned as (*Z*)-2-(2-(2,4-dinitrophenyl)-hydrazinylidene)-3-ethyl-4-methyl-2,3-dihydrothiazole and has the same spectral data as compound **3a** except that the benzyl group was replaced with ethyl, which gives two characteristic signals as triplet–quartet and appears in its ^{1}H NMR spectrum at δ_H = 1.28–1.38 (t, *J* = 3 Hz; 3H, ethyl-CH_3) and 3.88–3.98 ppm (q, *J* = 3 Hz; 2H, ethyl-CH_3) and was confirmed from its ^{13}C NMR spectrum, with two signals at δ_H = 12.98 (ethyl-CH_3) and 30.67 ppm (ethyl-CH_2).

Furthermore, the structures for the obtained products were confirmed via X-ray crystallography. Moreover, the X-ray measurements of compound **3b** showed that the molecule (except the C-atom of the ethyl substituent, C21) is virtual planar. The aromatic ring is coplanar with the thiazole ring, and the ethyl group has the hours conformation structure. The angle between the thiazole and the aromatic ring is 6.37(7)°, between the thiazole and the hydrazinylidene moiety is 2.98(14)°, and between the aromatic ring and the hydrazinylidene moiety is 6.56(9)° (angle between the L.S. planes of the moieties). In addition, the geometric structure around the exocyclic C=N has cissoid geometry concerning the thiazole *S*-atom and the hydrazo-group (Figure 4). The geometrical parameters (selected bond distance, bond angles, and dihedral angles; see Table 2) are in good correlation with the theoretical values.

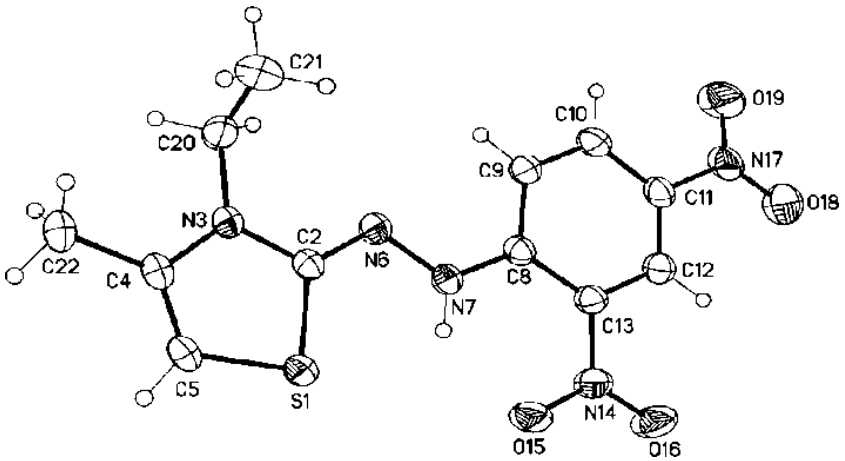

Figure 4. The crystal structure of *(Z)*-2-(2-(2,4-dinitrophenyl)hydrazinylidene)-3-ethyl-4-methyl-2,3-dihydrothiazole **3b**.

Table 2. Selected geometric parameters (Å, °) for **3b**.

S1—C5	1.742 (2)	N3—C4	1.394 (2)
S1—C2	1.7465 (19)	C4—C5	1.327 (3)
C2—N6	1.298 (2)	N6—N7	1.377 (2)
C2—N3	1.370 (2)	N7—C8	1.337 (2)
C5—S1—C2	90.45 (9)	N3—C4—C22	119.73 (19)
N6—C2—N3	121.44 (17)	C4—C5—S1	112.19 (14)

Table 2. *Cont.*

N6—C2—S1	128.53 (15)	C4—C5—H5	123.9
N3—C2—S1	110.03 (13)	S1—C5—H5	123.9
C2—N3—C4	113.80 (16)	C2—N6—N7	113.44 (16)
C2—N3—C20	120.49 (17)	C8—N7—N6	121.10 (17)
C4—N3—C20	125.43 (18)	C8—N7—H7	119.5
C5—C4—N3	113.50 (17)	N6—N7—H7	119.5
C5—C4—C22	126.76 (19)		
N3—C2—N6—N7	−179.55 (16)	N6—N7—C8—C9	1.6 (3)
S1—C2—N6—N7	0.1 (3)	N6—N7—C8—C13	−178.62 (16)
C2—N6—N7—C8	−174.03 (17)		

Based on the above results and the X-ray confirmation of our obtained products, the proposed mechanism is as follows. First, the nucleophilic attack of sulfur on the primary carbon atom results in the formation of the intermediate, **B** (S-alkylation), via the transition state, **A**. Another nucleophilic attack on the nitrogen atom on the carbonyl carbon gives the intermediate, **C**, followed by water molecule (dehydration) loss to give the target product. The reaction mechanism proceeds via the S_N2 reaction type (Scheme 2).

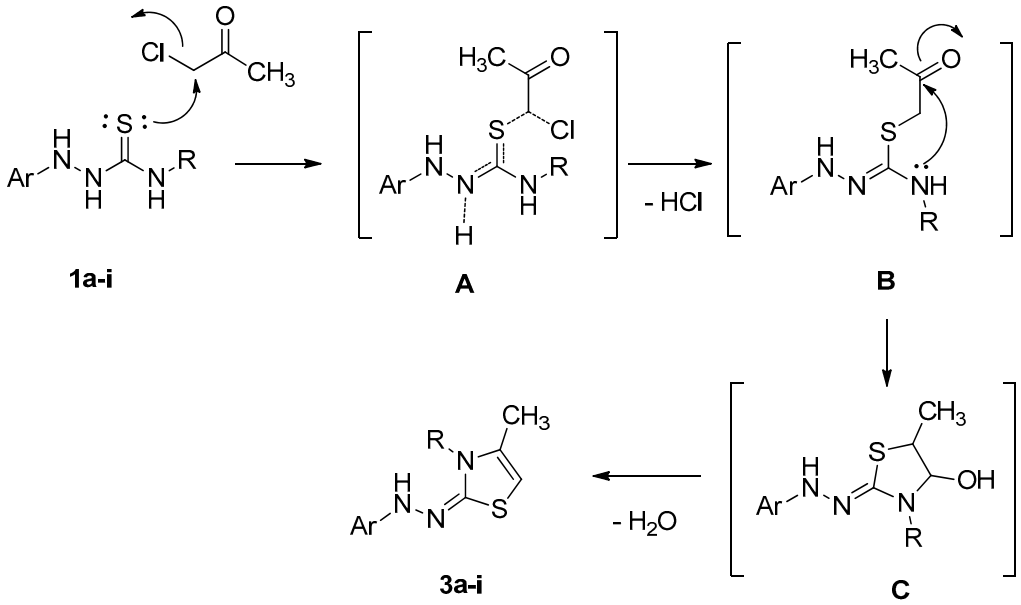

Scheme 2. The hypothesized mechanism for the synthesis of thiazole compounds **3a–i**.

2.2. Biology

2.2.1. Cell Viability Assay

The human mammary gland epithelial (MCF-10A) cell line was used to test the viability of the novel compounds [50,51]. After four days of incubation on MCF-10A cells, the vitality of compounds **3a–i** was determined using the MTT method. According to Table 3, the cell viability at 50 µM was greater than 87% for all tested agents, and none of the tested substances were cytotoxic.

Table 3. IC_{50} values of compounds **3a–i** against four cancer cell lines.

Compound	Cell Viability %	Antiproliferative Activity $IC_{50} \pm$ SEM (nM)				
		A-549	MCF-7	Panc-1	HT-29	Average
3a	89	45 ± 4	49 ± 4	48 ± 4	48 ± 4	48
3b	91	78 ± 7	82 ± 8	80 ± 8	80 ± 8	80
3c	90	50 ± 5	56 ± 5	54± 5	54 ± 5	54
3d	92	43 ± 4	47 ± 4	46 ± 4	46 ± 4	46
3e	87	71 ± 7	74 ± 7	72 ± 7	72 ± 7	72
3f	89	35 ± 3	40 ± 3	37 ± 3	37 ± 3	37
3g	90	58 ± 5	63 ± 6	60± 6	58 ± 5	60
3h	92	63 ± 6	68 ± 6	65 ± 6	65 ± 6	65
3i	95	84 ± 8	89 ± 8	86 ± 8	86 ± 8	86
Erlotinib	-	30 ± 3	40 ± 3	30 ± 3	30 ± 3	33

2.2.2. Antiproliferative Assay

The MTT assay was used to investigate the antiproliferative activity of **3a–i** against four human cancer cell lines: the colon cancer (HT-29) cell line, pancreatic cancer (Panc-1) cell line, lung cancer (A-549) cell line, and breast cancer (MCF-7) cell line, using erlotinib as the reference [52,53]. Table 3 shows the median inhibitory concentration (IC_{50}).

In general, the examined compounds **3a–i** displayed good antiproliferative activity, with average IC_{50} (GI_{50}) values ranging from 37 to 86 nM against the four tested human cancer cell lines, compared to the reference erlotinib (GI_{50} = 33 nM).

The most potent derivatives were compounds **3a**, **3c**, **3d**, and **3f**, with GI_{50} values ranging from 37 nM to 54 nM. Compound **3f** (Ar = 2,4-di-NO_2-C_6H_3, R = 4-CH_3-C_6H_5) was the most potent derivative of all synthesized compounds, with a GI_{50} value of 37 nM against the four tested human cancer cell lines, comparable to the reference erlotinib (GI_{50} = 33 nM). By replacing the *p*-tolyl group in compound **3f** with a cyclohexyl moiety, compound **3d** (Ar = 2,4-di-NO_2-C_6H_3, R = C_6H_{11}) was found to be the second-most potent compound, with a GI_{50} value of 46 nM, being 1.3-fold less potent than compound **3f**, demonstrating the importance of the *p*-tolyl moiety in antiproliferative activity.

The benzyl derivative, **3a** (Ar = 2,4-di-NO_2-C_6H_3, R = CH_2-C_6H_5), was less potent than **3f** and **3d**, with a GI_{50} value of 48 nM against the tested four cancer cell lines, while the allyl derivatives, **3c** (Ar = 2,4-di-NO_2-C_6H_3, R = $CH_2CH = CH_2$), showed moderate antiproliferative activity, with a GI_{50} value more than 50 nM. These findings show that allyl and benzyl groups are not preferred for the antiproliferative activity of scaffold A compounds **3a–f**.

The remaining scaffold A compounds, **3b** (Ar = 2,4-di-NO_2-C_6H_3, R = CH_2CH_3) and **3e** (Ar = 2,4-di-NO_2-C_6H_3, R = C_6H_5), had GI_{50} values of 80 nM and 72 nM, respectively. Compounds **3b** and **3e** were 2.2- and 2-fold less potent than **3f**, respectively, indicating weak antiproliferative activity (Table 3).

With GI_{50} values of 60 nM, 65 nM, and 86 nM, scaffold B compounds **3g**, **3h**, and **3i** demonstrated moderate-to-weak antiproliferative activity. Compound **3i** (Ar = *p*-CH_3-C_6H_4-SO_2, R = CH_2CH_3) was the least potent derivative of any of the synthesized compounds, with a GI_{50} value of 86 nM, which is less potent than its congeners, **3b** (scaffold A), which has the same structure, but the aryl moiety was *p*-CH_3-C_6H_4-SO_2, while in **3b** it was 2,4-di-NO_2-C_6H_3. These findings demonstrated that 2,4-di-NO_2-C_6H_3 significantly affects the antiproliferative action of the newly synthesized compounds.

2.2.3. Assay for EGFR Inhibition

The most promising antiproliferative compounds, **3a**, **3c**, **3d**, and **3f**, were further evaluated for their suppressive impact on EGFR as a probable target for their mechanism of action [50,54,55]. Table 4 compares the IC_{50} values to erlotinib, which worked as a control.

Table 4. IC_{50} of compounds **3a**, **3c**, **3d**, and **3f** against EGFR and $BRAF^{V600E}$.

Compound	EGFR Inhibition $IC_{50} \pm$ SEM (nM)	$BRAF^{V600E}$ Inhibition $IC_{50} \pm$ SEM (nM)
3a	93 ± 8	117 ± 10
3c	98 ± 9	126 ± 11
3d	91 ± 7	112 ± 10
3f	89 ± 7	93 ± 8
Erlotinib	80 ± 5	60 ± 5

The EGFR-TK inhibitory assay results matched the antiproliferative assay results, with the most potent derivatives, as antiproliferative agents, also being the most potent EGFR inhibitors. Compounds **3a**, **3c**, **3d**, and **3f** inhibited EGFR, with IC_{50} values ranging from 89 to 98 nM, but the tested compounds were less potent than erlotinib (IC_{50} = 80 nM). The most potent antiproliferative agent, compound **3f** (Ar = 2,4-di-NO_2-C_6H_3, R = 4-CH_3-C_6H_5), was also the most potent EGFR inhibitor, with an IC_{50} value of 89 ± 7, being 1.1-fold less potent than standard erlotinib.

Compounds **3a** (Ar = 2,4-di-NO_2-C_6H_3, R = CH_2-C_6H_5) and **3d** (Ar = 2,4-di-NO_2-C_6H_3, R = C_6H_{11}) ranked third and second in EGFR suppression, with IC_{50} values of 93 ± 8 and 91 ± 7 nM, respectively, being 1.15-fold less potent than erlotinib (IC_{50} = 80 ± 5 nM). These findings suggest that EGFR-TK could be a molecular target for the tested compound's antiproliferative action.

2.2.4. $BRAF^{V600E}$ Inhibitory Assay

Derivatives **3a**, **3c**, **3d**, and **3f** were further investigated as possible $BRAF^{V600E}$ inhibitors [56]. Table 4 displays the IC_{50} values compared to erlotinib, which was used as a control. According to Table 4, the evaluated derivatives had a promising $BRAF^{V600E}$ suppressive action, with IC_{50} values ranging from 93 to 126 nM, making them approximately 1.5-fold less effective than erlotinib (IC_{50} = 60 nM). Compound **3f**, the most potent derivative in the antiproliferative and EGFR suppressive assays, was also the most effective derivative as anti-$BRAF^{V600E}$ (IC_{50} = 93 ± 8 nM). These findings show that compound **3a** has potent antiproliferative activity as a dual EGFR/$BRAF^{V600E}$ inhibitor, implying that further structural modifications may be required to obtain a more potent lead compound for future development.

2.3. In Silico Study

AutoDock4.2.6 software was used to investigate the binding scores and poses of compounds **3a**, **3c**, **3d**, and **3f** against $BRAF^{V600E}$ and EGFR. The estimated docking features and scores are listed in Table 5. As tabulated in Table 5, all inspected compounds revealed good docking scores against $BRAF^{V600E}$ and EGFR targets**,** ranging from −7.8 to −8.7 kcal/mol and from −7.9 to −8.5 kcal/mol, respectively. The good docking scores of the inspected compounds toward $BRAF^{V600E}$ and EGFR may be imputed to their capability of forming H-bonds and vdW, pi-based, and hydrophobic interactions with the proximal residues within the active sites of the investigated targets (Table 5).

Table 5. Predicted binding features and docking scores for the top investigated compounds toward EGFR and $BRAF^{V600E}$.

Compound	EGFR		$BRAF^{V600E}$	
	Docking Scores (kcal/mol)	Binding Features	Docking Scores (kcal/mol)	Binding Features [a]
3a	−8.0	CYS773 (2.21 Å)	−8.4	LYS483 (2.15 Å), THR529 (2.38 Å), ASP594 (2.12 Å)
3c	−7.9	CYS773 (2.15 Å)	−7.8	LYS483 (2.13 Å) ASP594 (1.93 Å)
3d	−8.1	CYS773 (2.17 Å)	−8.5	LYS483 (1.93 Å), GLY596 (2.32 Å), THR529 (2.66 Å), ASP594 (2.14 Å)
3f	−8.5	CYS773 (2.18 Å)	−8.7	LYS483 (2.15 Å), THR529 (2.38 Å), ASP594 (2.12 Å)
Erlotinib	−8.6	MET769 (1.62 Å), CYS773 (1.91 Å)	−8.4	THR529 (2.07), CYS532 (2.02)

[a] Only hydrogen bonds are presented in Å.

Compound **3f** demonstrated superior docking scores of −8.7 and −8.5 kcal/mol against $BRAF^{V600E}$ and EGFR, respectively. Inspecting the docking mode of compound **3f** with the EGFR active site unveiled that this compound formed one H-bond with CYS773 (2.18 Å). Moreover, compound **3f** exhibited two carbon–hydrogen bonds with LEU768 and pi–anion interaction with ASP831. On the other hand, compound **3f**, complexed with $BRAF^{V600E}$, demonstrated three H-bonds with LYS483 (2.15 Å), THR529 (2.38 Å), and ASP594 (2.12 Å). Additionally, compound **3f** established pi–cation interaction with LYS483 and pi–pi stacking interaction with PHE583 and TRP531 residues (Figure 5).

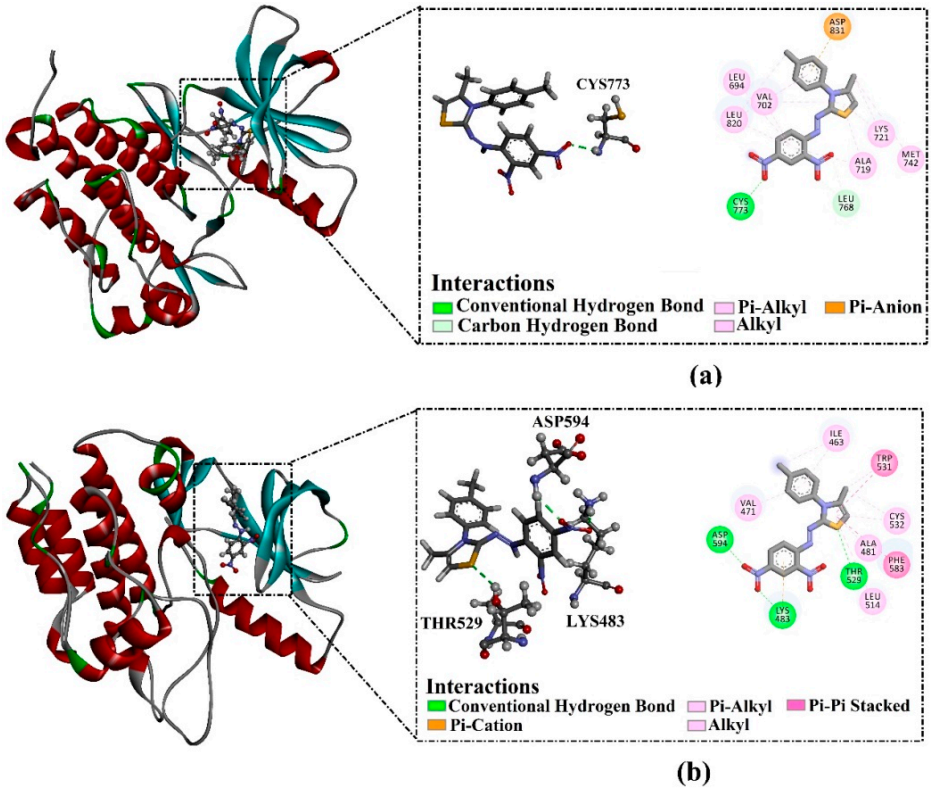

Figure 5. Molecular interactions of compound **3f** within (**a**) EGFR and (**b**) $BRAF^{V600E}$ active sites.

Compound **3d** showed the second-lowest docking score, with values of −8.5 and −8.1 kcal/mol against $BRAF^{V600E}$ and EGFR, respectively. Compound **3d** displayed one hydrogen bond with the CYS773 (2.17 Å) within the active site of EGFR. However, compound **3d** demonstrated four H-bonds with the LYS483 (1.93Å), GLY596 (2.32 Å), THR529 (2.66 Å), and ASP594 (2.14 Å) of $BRAF^{V600E}$.

Compound **3a** exposed the third-lowest docking score, with values of −8.4 and −8.0 kcal/mol against $BRAF^{V600E}$ and EGFR, respectively (Table 5). Compound **3a** made one H-bond with **the** CYS773 (2.21 Å) of EGFR, while compound **3a** exhibited three H-bonds with the LYS483 (2.15 Å), THR529 (2.38 Å), and ASP594 (2.12 Å) within the $BRAF^{V600E}$ binding pocket.

Compound **3c** also unveiled good docking scores, with values of −7.8 and −7.9 kcal/mol against $BRAF^{V600E}$ and EGFR, respectively (Table 5). Observably, compound **3c** established one H-bond with the CYS773 (2.15 Å) of EGFR and two H-bonds with the LYS483 (2.13 Å) and ASP593 (1.93 Å) of $BRAF^{V600E}$.

Erlotinib, a reference drug, showed docking scores of −8.4 and −8.6 kcal/mol toward $BRAFV^{600E}$ and EGFR, respectively (Table 5). From Table 5, erlotinib demonstrated two H-bonds with the CYS773 (1.91 Å) and MET769 (1.62 Å) within the EGFR binding pocket. In addition, erlotinib also displayed two H-bonds with CYS532 (2.02 Å) and THR529 (2.07 Å).

3. Material and Methods

3.1. Chemistry

General information: refer to Supplementary Information.

The starting materials, **1a–i**, were synthesized in accordance with the documented methods [46–48]

3.1.1. General Procedure of Synthesis of Trisubstituted Thiazoles **3a–i**

Method A

In a conical flask containing 10 mL ethyl acetate and two drops of Et_3N as a catalyst, 0.092 gm of chloroacetone were dissolved (**2**). To this mixture, 1 mmol of thiosemicarbazides **1a–i** in 10 mL ethyl acetate was added drop by drop while stirring. After addition was complete, the reaction mixture was stirred for 24 h. The reaction mixture was monitored with TLC. After the reaction was completed, the formed precipitate was filtered off and recrystallized from ethanol to afford products **3a–i** as fine crystals.

Method B

In a 50 mL round-bottom flask containing 20 mL absolute ethanol, a molar ratio (1:1) mixture of chloroacetone and substituted thiosemicarbazides **1a–i** was added. The flask was fitted with a condenser and was refluxed for 6–10 h. The reaction was monitored with TLC to assure the reaction completion. Then, the reaction mixture was cooled to room temperature, and the formed precipitate was filtered off and recrystallized from ethanol to afford products **3a–i**.

(Z)-3-Benzyl-2-(2-(2,4-Dinitrophenyl)Hydrazineylidene)-4-Methyl-2,3-Dihydrothiazole (**3a**)

This compound was found as red crystals from methanol in (98% and 85%) yield, with m.p., 215–217 °C; ^{1}H NMR (DMSO-d_6): δ 1.98 (s, 3H, CH_3), 5.00 (s, 2H, benzyl-CH_2), 6.42 (s, 1H, H-5), 7.10–8.28 (m, 6H, Ar-H), 7.96–8.01 (d, 1H, Ar-H), 8.68 (s, 1H, Ar-H), 10.38 (s, 1H, NH) ppm; ^{13}C NMR (DMSO-d_6): δ 13.7 (CH_3), 47.1 (benzyl-CH_2), 94.5 (C5), 115.5, 123.4, 126.6, 127.4, 127.7, 128.7 (Ar-CH), 129.5, 136.7, 136.7, 144.3 (Ar-C), 135.1 (C4), 164.1 (C2) ppm; IR: ν = 3286 (NH),3085 (Ar-CH), 2978 (ali-CH), 1609 (C=N), 1548 (Ar-C=C), 1399, 1117 (NO_2) cm^{-1}; MS (70 eV): *m/z* (%) = 385 (M^+, 30). *Anal. Calcd. For* $C_{17}H_{15}N_5O_4S$ (385.40): C, 52.98; H, 3.92; N, 18.17; S, 8.32. Found: C, 52.89; H, 3.81; N, 18.06; S, 8.23.

(Z)-2-(2-(2,4-Dinitrophenyl)Hydrazineylidene)-3-Ethyl-4-Methyl-2,3-Dihydrothiazole (**3b**)

This compound was found as red crystals from methanol in (99% and 84%) yield, with m.p., 176–177 °C; ^{1}H NMR (DMSO-d_6): δ 1.28–1.38 (t, 3H, J = 3, CH_3), 2.1 (s, 3H, CH_3), 3.88–3.98 (q, 2H, J = 3, CH_2), 6.14 (s, 1H, H-5), 7.48–7.54 (d, 1H, Ar-H), 8.22–8.28 (d, 1H, Ar-H), 8.82 (s, 1H, Ar-H), 10.46 (s, 1H, NH) ppm; ^{13}C NMR (DMSO-d_6): δ 12.9 (ethyl-CH_3), 13.4 (CH_3), 30.6 (ethyl-CH_2), 94.0 (C5), 115.5, 123.4, 127.6 (Ar-CH), 129.7, 136.8, 144.3 (Ar-C), 135.0 (C4), 163.6 (C2) ppm. IR: ν = 3115 (NH), 3078 (Ar-CH), 2988 (ali-CH), 1612 (C=N), 1557 (Ar-C=C), 1373, 1132 (NO_2). MS (70 eV): *m/z* (%) = 323 (M^+, 54). *Anal. Calcd. For* $C_{12}H_{13}N_5O_4S$ (323.33): C, 44.58; H, 4.05; N, 21.66; S, 9.92. Found: C, 44.46; H, 3.98; N, 21.57; S, 9.87.

(Z)-3-Allyl-2-(2-(2,4-Dinitrophenyl)Hydrazineylidene)-4-Methyl-2,3-Dihydrothiazole (**3c**)

This compound was found as red crystals from methanol in (96% and 83%) yield, with m.p. 197–198 °C; ^{1}H NMR (DMSO-d_6): δ 2.16 (s, 3H, CH_3), 4.52–4.58 (m, 2H, allyl-CH_2), 5.10–5.28 (m, 2H, allyl-CH_2=), 5.96–6.06 (m, 1H, allyl-CH=), 6.16 (s, 1H, H-5), 7.46–7.52 (d, 1H, Ar-H), 8.22–8.28 (d, 1H, Ar-H), 8.85 (s, 1H, Ar-H), 10.48 (s, 1H, NH) ppm; ^{13}C NMR (DMSO-d_6): δ 13.4 (CH_3), 46.1 (allyl-CH_2), 94.17 (C5), 116.6 (allyl-CH_2=), 115.6, 123.4, 128.3 (Ar-CH), 129.7, 136.9, 144.3 (Ar-C), 135.2 (C4), 136.9 (allyl-CH=), 164.4 (C2) ppm. IR: ν = 3105 (NH),3093 (Ar-CH), 2978 (ali-CH), 1606 (C=N), 1562 (Ar-C=C), 1374, 1206 (NO_2). MS (70 eV): *m/z* (%) = 335 (M^+, 93). *Anal. Calcd. For* $C_{13}H_{13}N_5O_4S$ (335.34): C, 46.56; H, 3.91; N, 20.88; S, 9.56. Found: C, 46.48; H, 3.85; N, 20.79; S, 9.47**.**

(Z)-3-Cyclohexyl-2-(2-(2,4-Dinitrophenyl)Hydrazineylidene)-4-Methyl-2,3-Dihydrothi-Azole (**3d**)

This compound was found as red crystals from methanol in (94% and 78%) yield, with m.p., 204–206 °C; ^{1}H NMR (DMSO-d_6): δ 1.34–1.46 (m, 10H, cyclohexyl-CH_2), 1.69–184 (m, 1H, cyclohexyl-CH), 2.21 (s, 3H, CH_3), 6.10 (s, 1H, H-5), 7.36–7.39 (d, 1H, Ar-H), 8.29–8.32 (dd, 1H, Ar-H), 8.84–8.85 (d, 1H, Ar-H), 10.48 (s, 1H, NH) ppm. IR: ν = 3110 (NH),3015 (Ar-CH), 2925 (ali-CH), 1608 (C=N), 1544 (Ar-C=C), 1323, 1034 (NO_2). MS (70 eV): *m/z* (%) = 377 (M^+, 80) *Anal. Calcd. For* $C_{16}H_{19}N_5O_4S$ (377.42): C, 50.92; H, 5.07; N, 18.56; S, 8.49. Found: C, 50.82; H, 4.93; N, 18.48; S, 8.43.

(Z)-2-(2-(2,4-Dinitrophenyl)Hydrazineylidene)-4-Methyl-3-Phenyl-2,3-Dihydrothiazole (**3e**)

This compound was found as red crystals from methanol in (94% and 83%) yield, with m.p., 231–233 °C; ^{1}H NMR (DMSO-d_6): δ 1.80 (s, 3H, CH_3), 6.34 (s, 1H, H-5), 7.14–7.17 (d, 1H, Ar-H), 7.49–7.36 (m, 5H, Ar-H), 8.26–8.30 (dd, 1H, Ar-H), 8.85–8.86 (d, 1H, Ar-H), 10.47 (s, 1H, NH) ppm; ^{13}C NMR (DMSO-d_6): δ 14.5 (CH_3), 95.3 (C5), 115.5, 123.3, 127.8, 128.5, 128.9, 129.6 (Ar-CH), 129.7, 136.2, 136.5, 144.5 (Ar-C), 135.2 (C4), 165.5 (C2) ppm; IR: ν = 3226 (NH), 3118 (Ar-CH), 2975 (ali-CH), 1603 (C=N),1555 (Ar-C=C), 1355, 1133 (NO_2) cm^{-1}; MS (70 eV): *m/z* (%) = 371 (M^+, 8). *Anal. Calcd. For* $C_{16}H_{13}N_5O_4S$ (371.37): C, 51.75; H, 3.53; N, 18.86; S, 8.63. Found: C, 51.68; H, 3.49; N, 18.79; S, 8.52.

(Z)-2-(2-(2,4-Dinitrophenyl)Hydrazineylidene)-4-Methyl-3-(p-Tolyl)-2,3-Dihydrothi-Azole (**3f**)

This compound was found as red crystals from methanol in (92% and 86%) yield, with m.p., 198–199 °C; ^{1}H NMR (DMSO-d_6): δ 1.87 (s, 3H, CH_3), 2.40 (s, 3H, tolyl-CH_3), 6.32 (s, 1H, H-5), 7.14–7.17 (d, 1H, Ar-H), 7.35–7.39 (m, 4H, Ar-H), 8.19–8.24 (dd, 1H, Ar-H), 8.81–8.83 (d, 1H, Ar-H), 10.47 (s, 1H, NH) ppm; ^{13}C NMR (DMSO-d_6): δ 14.5 (CH_3), 20.7 (tolyl-CH_3), 95.1 (C5), 115.5, 123.6, 127.8, 128.2, 129.7 (Ar-CH), 130.1, 134.1, 137.5, 138.4, 144.4 (Ar-C), 136.1 (C4), 165.4 (C2) ppm. IR: ν = 3226 (NH),3088 (Ar-CH), 2945 (ali-CH), 1607 (C=N), 1559 (Ar-C=C), 1383, 1172 (NO_2). MS (70 eV): *m/z* (%) = 385 (M^+, 13). *Anal. Calcd. For* $C_{17}H_{15}N_5O_4S$ (385.40): C, 52.98; H, 3.92; N, 18.17; S, 8.32. Found: C, 52.89; H, 3.87; N, 18.11; S, 8.25.

(Z)-4-Methyl-N′-(4-Methyl-3-Phenylthiazol-2(3H)-Ylidene) Benzenesulfonohydrazide (**3g**)

This compound was found as pale-yellow crystals from methanol in (90% and 83%) yield, with m.p., 193–194 °C; ^{1}H NMR (DMSO-d_6): δ 2.13 (s, 3H, CH_3), 2.30 (s, 3H, tolyl-CH_3), 5.93 (s, 1H, H-5), 6.40 (d, 2H, tolyl-H-*m*), 6.93 (m, 1H, Ar-H), 7.19 (m, 2H, Ar-H), 7.31 (d, 2H, tolyl-H-*o*), 7.69 (m, 2H, Ar-H), 10.92 (s, 1H, NH) ppm; ^{13}C NMR (DMSO-d_6): δ 13.8 (CH_3), 20.9 (tolyl-CH_3), 91.0 (C5), 120.5, 122.9, 127.7, 128.9, 129.2 (Ar-CH), 137.6, 143.5, 148.5 (Ar-C), 136.0 (C4), 155.2 (C2) ppm. IR: ν = 3130 (NH),3062 (Ar-CH), 2920 (ali-CH), 1595 (C=N), 1561 (Ar-C=C). MS (70 eV): *m/z* (%) = 359 (M^+, 100). *Anal. Calcd. For* $C_{17}H_{17}N_3O_2S_2$ (359.46): C, 56.80; H, 4.77; N, 11.69; S, 17.84. Found: C, 56.73; H, 4.69; N, 11.63; S, 17.73.

(Z)-N′-(3-Allyl-4-Methylthiazol-2(3H)-Ylidene)-4-Methyl Benzenesulfonohydrazide (**3h**)

This compound was found as pale-yellow crystals from methanol in (89% and 83%) yield, with m.p., 236–238 °C. IR: ν = 3115 (NH),3078 (Ar-CH), 2988 (ali-CH), 1612 (C=N), 1557 (Ar-C=C), 1373, 1132 (NO_2) cm^{-1}. MS (70 eV): *m/z* (%) = 323 (M^+, 100). *Anal. Calcd. For* $C_{14}H_{17}N_3O_2S_2$ (323.43): C, 51.99; H, 5.30; N, 12.99; S, 19.83. Found: C, 51.91; H, 5.23; N, 12.92; S, 19.78.

(Z)-N′-(3-Ethyl-4-Methylthiazol-2(3H)-Ylidene)-4-Methyl Benzenesulfonohydrazide (**3i**)

This compound was found as pale-yellow crystals from methanol in (87% and 78%) yield, with m.p., 236–238 °C. ^{1}H NMR (DMSO-d_6): δ 1.26–1.39 (t, 3H, CH_3), 2.12 (s, 3H, CH_3), 3.80–3.96 (q, 2H, CH_2), 5.91 (s, 1H, H-5), 6.42 (d, 2H, Ar-H), 7.13 (d, 2H, Ar-H), 10.89 ppm (s, 1H, NH). IR: ν = 3112 (NH), 3044 (Ar-CH), 2946 (ali-CH), 1613 (C=N), 1545 (Ar-C=C), cm^{-1};. MS (70 eV): *m/z* (%) = 311 (M^+, 65). *Anal. Calcd. For* $C_{13}H_{17}N_3O_2S_2$ (311.42): C, 50.14; H, 5.50; N, 13.49; O, 10.27; S, 20.59. Found: C, 50.09; H, 5.41; N, 13.39; S, 20.53.

3.1.2. Crystal X-ray Structure Determination of **3b**

Compound **3b** was obtained as single crystals by recrystallization from methanol. Bruker D8 Venture diffractometer with Photon II detector at 298(2) K using Cu-Kα radiation (λ = 1.54178 Å) was used to study the single-crystal X-ray diffraction. Moreover, we used dual space methods (SHELXT for **5a**) [57,58] for the structure solution, and refinement was carried out using SHELXL-2014 (full-matrix least-squares on F^2) [59]. Hydrogen atoms were localized by difference electron density determination and refined using a riding model. Semi-empirical absorption corrections and a general RIGU restraint were applied.

3b: red crystals, $C_{12}H_{13}N_5O_4S$, M_r = 323.33, crystal size 0.20 × 0.04 × 0.02 mm, triclinic, space group *P-1* (No. 2), *a* = 7.0981(2) Å, *b* = 8.2929(2) Å, *c* = 13.0081(4) Å, α = 101.598(1)°, β = 103.030(1)°, γ = 92.366(1)°, *V* = 727.74(4) $Å^3$, *Z* = 2, ρ = 1.476 Mg/m^{-3}, μ(Cu-K_α) = 2.24 mm^{-1}, *F*(000) = 336, *T* = 298 K, $2\theta_{max}$ = 144.4°, 13,774 reflections, of which 2874 were independent (R_{int} = 0.058), 200 parameters, 165 restraints (see cif-file for details), R_1 = 0.063 (for 2692 I > 2σ(I)), wR_2 = 0.170 (all data), *S* = 1.07, largest diff. peak/hole = 0.78/−0.40 e $Å^{-3}$.

CCDC 2265616 (**3b**) contains the supplementary crystallographic data for this paper. These data can be obtained free of charge from the Cambridge Crystallographic Data Centre via www.ccdc.cam.ac.uk/data_request/cif (accessed on 24 June 2023).

3.2. Biology

3.2.1. Cell Viability Assay

The human mammary gland epithelial (MCF-10A) cell line was used to test the viability of compounds **3a**–**i** [50,60]. See Supplementary Information.

3.2.2. Antiproliferative Assay

The MTT assay was used to investigate **3a**–**i**'s antiproliferative activity versus four human cancer cell lines: colon cancer (HT-29) cell line, pancreatic cancer (Panc-1) cell line, lung cancer (A-549) cell line, and breast cancer (MCF-7) cell line, using erlotinib as the reference [52,53]. See Supplementary Information.

3.2.3. EGFR Inhibitory Assay

Compounds **3a**, **3c**, **3d**, and **3f** were further evaluated for their suppressive effect versus EGFR as a probable molecular target for their mechanism of action [50,54]. See Supplementary Information.

3.2.4. $BRAF^{V600E}$ Inhibitory Assay

Derivatives **3a**, **3c**, **3d**, and **3f** were further investigated as possible $BRAF^{V600E}$ inhibitors [61]. See Supplementary Information.

3.3. In Silico Study

The crystal structures of $BRAF^{V600E}$ and EGFR, with PDB codes 3OG7 [62] and 1M17 [63], respectively, were prepared for all docking computations. All heteroatoms, water molecules, ligands, and ions were removed to prepare the PDB files. Modeler software was applied to construct all missing amino acids [64,65]. The protonation state of titratable residues of the investigated targets was estimated using PropKa software at pH 7.0 [66]. The 3D structure of the investigated compounds was energetically minimized using the MMFF94S force field within SZYBKI software [67,68].

For docking computations, AutoDock4.2.6 software was utilized [69]. All docking parameters were set to default values, except *GA* run and energy evaluation, which were 250 and 25,000,000, respectively. The active site of the investigated targets was inspected by a grid box with a size of 50 Å × 50 Å × 50 Å. The grid maps were generated using the AutoGrid program with a spacing of 0.375 Å. Gasteiger–Marsili method was employed to assign the atomic charges of the chemical compounds [70]. Discovery Studio module of Biovia software 17.1.0.115 was utilized to visualize all drug–protein interactions [71].

4. Conclusions

Using simple interactions between thiosemicarbazides and chloroacetone, a novel set of heterocycles with thiazole rings was developed. All obtained derivatives were validated using various spectral data such as IR, NMR, mass spectrometry, elemental analysis, and X-ray crystallography. The newly synthesized compounds, **3a**–**i**, were evaluated against a panel of four human cancer cell lines, with compounds **3a**, **3c**, **3d**, and **3f** being the most potent variants. The in vitro assay results demonstrated that compound 3f possesses potent antiproliferative activity as a dual EGFR/$BRAF^{V600E}$ inhibitor, signaling that further structural modifications may be needed to establish a more potent lead molecule for future development. Finally, the docking analysis results showed that all inspected compounds revealed good docking scores toward $BRAF^{V600E}$ and EGFR.

Supplementary Materials: The following supporting information can be downloaded at https://www.mdpi.com/article/10.3390/ph16071014/s1. Figure S1: The crystal structure of (Z)-2-(2-(2,4-dinitrophenyl)hydrazineylidene)-3-ethyl-4-methyl-2,3-dihydrothiazole **3b**; Figures S2–S32: IR and NMR analysis of the structure assignment for all obtained products **3a**–**i**.

Author Contributions: B.G.M.Y., E.M.E.-S., A.A.H. and H.N.T.: conceptualization, methodology, writing, editing, and revision. L.H.A.-W.: writing, editing, and revision. S.B.: writing and editing. M.N.: X-ray analysis. M.A.A.I.: docking study. All authors have read and agreed to the published version of the manuscript.

Funding: This research was funded by Princess Nourah Bint Abdulrahman University Researchers Supporting Project Number PNURSP2023R3, Princess Nourah Bint Abdulrahman University, Riyadh, Saudi Arabia.

Institutional Review Board Statement: Not applicable.

Informed Consent Statement: Not applicable.

Data Availability Statement: Data is contained within the article and Supplementary Material.

Acknowledgments: The authors extend their appreciation to Princess Nourah Bint Abdulrahman University Researchers Supporting Project Number PNURSP2023R3, Princess Nourah Bint Abdulrahman University, Riyadh, Saudi Arabia. The authors also acknowledge support by the KIT-Publication Fund of the Karlsruhe Institute of Technology.

Conflicts of Interest: The authors declare no conflict of interest.

References

1. Falzone, L.; Salomone, S.; Libra, M. Evolution of Cancer Pharmacological Treatments at the Turn of the Third Millennium. *Front. Pharmacol.* **2018**, *9*, 1300. [CrossRef] [PubMed]
2. Bin Emran, T.; Shahriar, A.; Mahmud, A.R.; Rahman, T.; Abir, M.H.; Siddiquee, M.F.-R.; Ahmed, H.; Rahman, N.; Nainu, F.; Wahyudin, E.; et al. Multidrug Resistance in Cancer: Understanding Molecular Mechanisms, Immunoprevention and Therapeutic Approaches. *Front. Oncol.* **2022**, *12*, 2581. [CrossRef] [PubMed]
3. Housman, G.; Byler, S.; Heerboth, S.; Lapinska, K.; Longacre, M.; Snyder, N.; Sarkar, S. Drug Resistance in Cancer: An Overview. *Cancers* **2014**, *6*, 1769–1792. [CrossRef] [PubMed]
4. Bhullar, K.S.; Lagarón, N.O.; McGowan, E.M.; Parmar, I.; Jha, A.; Hubbard, B.P.; Rupasinghe, H.P.V. Kinase-targeted cancer therapies: Progress, challenges and future directions. *Mol. Cancer* **2018**, *17*, 48. [CrossRef]
5. Nishal, S.; Jhawat, V.; Gupta, S.; Phaugat, P. Utilization of kinase inhibitors as novel therapeutic drug targets: A review. *Oncol. Res.* **2023**, *30*, 221–230. [CrossRef]
6. Al-Wahaibi, L.H.; Gouda, A.M.; Abou-Ghadir, O.F.; Salem, O.I.; Ali, A.T.; Farghaly, H.S.H.; Abdelrahman, M.H.; Trembleau, L.; Abdu-Allah, H.H.; Youssif, B.G. Design and synthesis of novel 2,3-dihydropyrazino[1,2-a]indole-1,4-dione derivatives as antiproliferative EGFR and BRAFV600E dual inhibitors. *Bioorg. Chem.* **2020**, *104*, 104260. [CrossRef]
7. Jarvinen, T.A.; Liu, E.T. Simultaneous amplification of HER-2 (ERBB2) and topoisomerase IIα (TOP2A) genes-molecular basis for combination chemotherapy in cancer. *Curr. Cancer Drug Targets* **2006**, *6*, 579–602. [CrossRef]
8. Gurunathan, S.; Kang, M.-H.; Qasim, M.; Kim, J.-H. Nanoparticle-Mediated Combination Therapy: Two-in-One Approach for Cancer. *Int. J. Mol. Sci.* **2018**, *19*, 3264. [CrossRef]
9. Lehár, J.; Krueger, A.S.; Avery, W.; Heilbut, A.M.; Johansen, L.M.; Price, E.R.; Rickles, R.J.; Iii, G.F.S.; Staunton, J.E.; Jin, X.; et al. Synergistic drug combinations tend to improve therapeutically relevant selectivity. *Nat. Biotechnol.* **2009**, *27*, 659–666. [CrossRef]
10. Kendall, J.M. Designing a research project: Randomised controlled trials and their principles. *Emerg. Med. J.* **2003**, *20*, 164–168. [CrossRef]
11. Lim, Z.-F.; Ma, P.C. Emerging insights of tumor heterogeneity and drug resistance mechanisms in lung cancer targeted therapy. *J. Hematol. Oncol.* **2019**, *12*, 134. [CrossRef]
12. Hoelder, S.; Clarke, P.A.; Workman, P. Discovery of small molecule cancer drugs: Successes, challenges and opportunities. *Mol. Oncol.* **2012**, *6*, 155–176. [CrossRef] [PubMed]
13. Shah, K.N.; Bhatt, R.; Rotow, J.; Rohrberg, J.; Olivas, V.; Wang, V.E.; Hemmati, G.; Martins, M.M.; Maynard, A.; Kuhn, J.; et al. Aurora kinase A drives the evolution of resistance to third-generation EGFR inhibitors in lung cancer. *Nat. Med.* **2019**, *25*, 111–118. [CrossRef] [PubMed]
14. Wu, C.-P.; Murakami, M.; Wu, Y.-S.; Lin, C.-L.; Li, Y.-Q.; Huang, Y.-H.; Hung, T.-H.; Ambudkar, S.V. The multitargeted tyrosine kinase inhibitor SKLB610 resensitizes ABCG2-overexpressing multidrug-resistant cancer cells to chemotherapeutic drugs. *Biomed. Pharmacother.* **2022**, *149*, 112922. [CrossRef]
15. Kanojia, D.; Garg, M.; Martinez, J.; MT, A.; Luty, S.B.; Doan, N.B.; Said, J.W.; Forscher, C.; Tyner, J.W.; Koeffler, H.P. Kinase profiling of liposarcomas using RNAi and drug screening assays identified druggable targets. *J. Hematol. Oncol.* **2017**, *10*, 173. [CrossRef]
16. Sun, D.; Zhao, Y.; Zhang, S.; Zhang, L.; Liu, B.; Ouyang, L. Dual-target kinase drug design: Current strategies and future directions in cancer therapy. *Eur. J. Med. Chem.* **2020**, *188*, 112025. [CrossRef]
17. Zou, X.; Tang, X.-Y.; Qu, Z.-Y.; Sun, Z.-W.; Ji, C.-F.; Li, Y.-J.; Guo, S.-D. Targeting the PDGF/PDGFR signaling pathway for cancer therapy: A review. *Int. J. Biol. Macromol.* **2022**, *202*, 539–557. [CrossRef]
18. Ho, C.-C.; Liao, W.-Y.; Lin, C.-A.; Shih, J.-Y.; Yu, C.-J.; Yang, J.C.-H. Acquired BRAF V600E Mutation as Resistant Mechanism after Treatment with Osimertinib. *J. Thorac. Oncol. Off. Publ. Int. Assoc. Study Lung Cancer* **2017**, *12*, 567–572. [CrossRef] [PubMed]
19. Nana, F.A.; Ocak, S. Targeting *BRAF* Activation as Acquired Resistance Mechanism to EGFR Tyrosine Kinase Inhibitors in *EGFR*-Mutant Non-Small-Cell Lung Cancer. *Pharmaceutics* **2021**, *13*, 1478. [CrossRef]
20. Hyman, D.M.; Puzanov, I.; Subbiah, V.; Faris, J.E.; Chau, I.; Blay, J.-Y.; Wolf, J.; Raje, N.S.; Diamond, E.L.; Hollebecque, A.; et al. Vemurafenib in Multiple Nonmelanoma Cancers with *BRAF* V600 Mutations. *N. Engl. J. Med.* **2015**, *373*, 726–736. [CrossRef]
21. Amodio, V.; Yaeger, R.; Arcella, P.; Cancelliere, C.; Lamba, S.; Lorenzato, A.; Arena, S.; Montone, M.; Mussolin, B.; Bian, Y.; et al. EGFR Blockade Reverts Resistance to KRASG12C Inhibition in Colorectal Cancer. *Cancer Discov.* **2020**, *10*, 1129–1139. [CrossRef] [PubMed]
22. Prahallad, A.; Sun, C.; Huang, S.; Di Nicolantonio, F.; Salazar, R.; Zecchin, D.; Beijersbergen, R.L.; Bardelli, A.; Bernards, R. Unresponsiveness of colon cancer to BRAF(V600E) inhibition through feedback activation of EGFR. *Nature* **2012**, *483*, 100–103. [CrossRef] [PubMed]

23. Desai, J.; Markman, B.; Ananda, S.; Tebbutt, N.C.; Michael, M.; Solomon, B.J.; McArthur, G.A.; Tie, J.; Gibbs, P.; Ritchie, D.; et al. A phase I/II trial of combined BRAF and EGFR inhibition in patients (pts) with BRAF V600E mutated (BRAFm) metastatic colorectal (mCRC): The EViCT (Erlotinib and Vemurafenib in Combination Trial) study. *J. Clin. Oncol.* **2017**, *35*, 3557. [CrossRef]
24. Liu, H.; Nazmun, N.; Hassan, S.; Liu, X.; Yang, J. BRAF mutation and its inhibitors in sarcoma treatment. *Cancer Med.* **2020**, *9*, 4881–4896. [CrossRef]
25. Corcoran, R.B.; André, T.; Atreya, C.E.; Schellens, J.H.; Yoshino, T.; Bendell, J.C.; Hollebecque, A.; McRee, A.J.; Siena, S.; Middleton, G. Combined BRAF, EGFR, and MEK Inhibition in Patients with BRAFV600E-Mutant Colorectal Can-cerBRAF/EGFR/MEK Inhibition in BRAFV600E Colorectal Cancer. *Cancer Discov.* **2018**, *8*, 428–443. [CrossRef]
26. Bahrami, A.; Hesari, A.; Khazaei, M.; Hassanian, S.M.; Ferns, G.A.; Avan, A. The therapeutic potential of targeting the BRAF mutation in patients with colorectal cancer. *J. Cell Physiol.* **2017**, *233*, 2162–2169. [CrossRef]
27. Lozynskyi, A.; Zimenkovsky, B.; Lesyk, R. Synthesis and anticancer activity of new thiopyrano [2, 3-d] thiazoles based on cinnamic acid amides. *Sci. Pharm.* **2014**, *82*, 723–734. [CrossRef] [PubMed]
28. Janowska, S.; Khylyuk, D.; Bielawska, A.; Szymanowska, A.; Gornowicz, A.; Bielawski, K.; Noworól, J.; Mandziuk, S.; Wujec, M. New 1,3,4-Thiadiazole Derivatives with Anticancer Activity. *Molecules* **2022**, *27*, 1814. [CrossRef]
29. Arshad, M.F.; Alam, A.; Alshammari, A.A.; Alhazza, M.B.; Alzimam, I.M.; Alam, A.; Mustafa, G.; Ansari, S.; Alotaibi, A.M.; Alotaibi, A.A.; et al. Thiazole: A Versatile Standalone Moiety Contributing to the Development of Various Drugs and Biologically Active Agents. *Molecules* **2022**, *27*, 3994. [CrossRef]
30. Franchetti, P.; Cappellacci, L.; Grifantini, M.; Barzi, A.; Nocentini, G.; Yang, H.; O'Connor, A.; Jayaram, H.N.; Carrell, C.; Goldstein, B.M. Furanfurin and Thiophenfurin: Two Novel Tiazofurin Analogs. Synthesis, Structure, Antitumor Activity, and Interactions with Inosine Monophosphate Dehydrogenase. *J. Med. Chem.* **1995**, *38*, 3829–3837. [CrossRef]
31. Li, X.; He, Y.; Ruiz, C.H.; Koenig, M.; Cameron, M.D. Characterization of Dasatinib and Its Structural Analogs as CYP3A4 Mechanism-Based Inactivators and the Proposed Bioactivation Pathways. *Drug Metab. Dispos.* **2009**, *37*, 1242–1250. [CrossRef] [PubMed]
32. Hughes, T.P.; Laneuville, P.; Rousselot, P.; Snyder, D.S.; Rea, D.; Shah, N.P.; Paar, D.; Abruzzese, E.; Hochhaus, A.; Lipton, J.H.; et al. Incidence, outcomes, and risk factors of pleural effusion in patients receiving dasatinib therapy for Philadelphia chromosome-positive leukemia. *Haematologica* **2018**, *104*, 93–101. [CrossRef] [PubMed]
33. Hu-Lieskovan, S.; Mok, S.; Moreno, B.H.; Tsoi, J.; Robert, L.; Goedert, L.; Pinheiro, E.M.; Koya, R.C.; Grae-ber, T.G.; Comin-Anduix, B. Improved antitumor activity of immunotherapy with BRAF and MEK inhibitors in BRAF V600E melanoma. *Sci. Transl. Med.* **2015**, *7*, 279ra41. [CrossRef]
34. Argenziano, G.; Banzi, C.; De Blasio, S.; Lallas, A.; Longo, C.; Moscarella, E.; Alfano, R. Dabrafenib: A new opportunity for the treatment of BRAF V600-positive melanoma. *OncoTargets Ther.* **2016**, *ume 9*, 2725–2733. [CrossRef]
35. Abdel-Maksoud, M.S.; Kim, M.-R.; El-Gamal, M.I.; El-Din, M.M.G.; Tae, J.; Choi, H.S.; Lee, K.-T.; Yoo, K.H.; Oh, C.-H. Design, synthesis, in vitro antiproliferative evaluation, and kinase inhibitory effects of a new series of imidazo [2, 1-b] thiazole derivatives. *Eur. J. Med. Chem.* **2015**, *95*, 453–463. [CrossRef] [PubMed]
36. Aly, A.A.; Alshammari, M.B.; Ahmad, A.; Gomaa, H.A.M.; Youssif, B.G.M.; Bräse, S.; Ibrahim, M.A.A.; Mohamed, A.H. Design, synthesis, docking and mechanistic studies of new thiazolyl/thiazolidinylpyrimidine-2,4-dione antiproliferative agents. *Arab. J. Chem.* **2023**, *16*, 104612. [CrossRef]
37. Ballatore, C.; Huryn, D.M.; Smith, A.B. Carboxylic Acid (Bio)Isosteres in Drug Design. *Chemmedchem* **2013**, *8*, 385–395. [CrossRef] [PubMed]
38. Ammazzalorso, A.; De Filippis, B.; Giampietro, L.; Amoroso, R. *N*-acylsulfonamides: Synthetic routes and biological potential in medicinal chemistry. *Chem. Biol. Drug Des.* **2017**, *90*, 1094–1105. [CrossRef]
39. Ghorab, M.M.; Alsaid, M.S.; El-Gaby, M.S.; Safwat, N.A.; Elaasser, M.M.; Soliman, A.M. Biological evaluation of some new N-(2,6-dimethoxypyrimidinyl) thioureido benzenesulfonamide derivatives as potential antimicrobial and anticancer agents. *Eur. J. Med. Chem.* **2016**, *124*, 299–310. [CrossRef]
40. Alaoui, S.; Dufies, M.; Driowya, M.; Demange, L.; Bougrin, K.; Robert, G.; Auberger, P.; Pagès, G.; Benhida, R. Synthesis and anti-cancer activities of new sulfonamides 4-substituted-triazolyl nucleosides. *Bioorg. Med. Chem. Lett.* **2017**, *27*, 1989–1992. [CrossRef]
41. Wan, Y.; Fang, G.; Chen, H.; Deng, X.; Tang, Z. Sulfonamide derivatives as potential anti-cancer agents and their SARs elucidation. *Eur. J. Med. Chem.* **2021**, *226*, 113837. [CrossRef]
42. Al-Wahaibi, L.H.; Mahmoud, M.A.; Mostafa, Y.A.; Raslan, A.E.; Youssif, B.G. Novel piperine-carboximidamide hybrids: Design, synthesis, and antiproliferative activity via a multi-targeted inhibitory pathway. *J. Enzym. Inhib. Med. Chem.* **2023**, *38*, 376–386. [CrossRef] [PubMed]
43. Gomaa, H.A.; Shaker, M.E.; Alzarea, S.I.; Hendawy, O.; Mohamed, F.A.; Gouda, A.M.; Ali, A.T.; Morcoss, M.M.; Abdelrahman, M.H.; Trembleau, L.; et al. Optimization and SAR investigation of novel 2,3-dihydropyrazino[1,2-a]indole-1,4-dione derivatives as EGFR and BRAFV600E dual inhibitors with potent antiproliferative and antioxidant activities. *Bioorg. Chem.* **2022**, *120*, 105616. [CrossRef]
44. Mohassab, A.M.; Hassan, H.A.; Abdelhamid, D.; Gouda, A.M.; Youssif, B.G.M.; Tateishi, H.; Fujita, M.; Otsuka, M.; Abdel-Aziz, M. Design and synthesis of novel quinoline/chalcone/1,2,4-triazole hybrids as potent antiproliferative agent targeting EGFR and BRAFV600E kinases. *Bioorg. Chem.* **2020**, *106*, 104510. [CrossRef] [PubMed]

45. Youssif, B.G.; Abdelrahman, M.H.; Abdelazeem, A.H.; Ibrahim, H.M.; Salem, O.I.; Mohamed, M.F.; Treambleau, L.; Bukhari, S.N.A. Design, synthesis, mechanistic and histopathological studies of small-molecules of novel in-dole-2-carboxamides and pyrazino [1, 2-a] indol-1 (2H)-ones as potential anticancer agents effecting the reactive oxygen species production. *Eur. J. Med. Chem.* **2018**, *146*, 260–273. [CrossRef]
46. Noto, R.; Meo, P.L.; Gruttadauria, M.; Werber, G. A quantitative study of substituent effects on oxidative cycliza-tion of some 2-aryl-substituted aldehyde thiosemicarbazones induced by ferric chloride and cupric perchlorate. *J. Heterocycl. Chem.* **1999**, *36*, 667–674. [CrossRef]
47. Krishna, P.M.; Reddy, N.G.; Harish, B.; Patil, Y.P.; Nethaji, M. Synthesis, structural studies, molecular docking and DNA binding studies of 4N-substituted hydrazinecarbothioamides. *J. Mol. Struct.* **2019**, *1175*, 97–104. [CrossRef]
48. Munir, R.; Zia-ur-Rehman, M.; Murtaza, S.; Zaib, S.; Javid, N.; Awan, S.J.; Iftikhar, K.; Athar, M.M.; Khan, I. Micro-wave-Assisted Synthesis of (Piperidin-1-yl) quinolin-3-yl) methylene) hydrazinecarbothioamides as Potent Inhibitors of Cholinesterases: A Biochemical and In silico Approach. *Molecules* **2021**, *26*, 656. [CrossRef]
49. Basri, R.; Ullah, S.; Halim, S.A.; Alharthy, R.D.; Rauf, U.; Khan, A.; Hussain, J.; Al-Ghafri, A.; Al-Harrasi, A.; Shafiq, Z. Synthesis, biological evaluation, and molecular docking study of chromen-linked hydrazine carbothioamides as potent α-glucosidase inhibitors. *Drug Dev. Res.* **2023**. [CrossRef]
50. Al-Wahaibi, L.H.; Mostafa, Y.A.; Abdelrahman, M.H.; El-Bahrawy, A.H.; Trembleau, L.; Youssif, B.G.M. Synthesis and Biological Evaluation of Indole-2-Carboxamides with Potent Apoptotic Antiproliferative Activity as EGFR/CDK2 Dual Inhibitors. *Pharmaceuticals* **2022**, *15*, 1006. [CrossRef]
51. Riss, T.L.; Moravec, R.A.; Niles, A.L.; Duellman, S.; Benink, H.A.; Worzella, T.J.; Minor, L. Cell Viability Assays, Assay Guidance Manual [Internet]. 2016. Available online: https://www.ncbi.nlm.nih.gov/books/NBK144065/ (accessed on 11 July 2023).
52. Mahmoud, M.A.; Mohammed, A.F.; Salem, O.I.; Gomaa, H.A.; Youssif, B.G. New 1, 3, 4-oxadiazoles linked with the 1, 2, 3-triazole moiety as antiproliferative agents targeting the EGFR tyrosine kinase. *Arch. Pharm.* **2022**, *355*, 2200009. [CrossRef] [PubMed]
53. Mahmoud, M.A.; Mohammed, A.F.; Salem, O.I.; Rabea, S.M.; Youssif, B.G. Design, synthesis, and antiproliferative properties of new 1,2,3-triazole-carboximidamide derivatives as dual EGFR/VEGFR-2 inhibitors. *J. Mol. Struct.* **2023**, *1282*, 135165. [CrossRef]
54. Mohamed, F.A.; Gomaa, H.A.; Hendawy, O.; Ali, A.T.; Farghaly, H.S.; Gouda, A.M.; Abdelazeem, A.H.; Ab-delrahman, M.H.; Trembleau, L.; Youssif, B.G. Design, synthesis, and biological evaluation of novel EGFR inhibitors con-taining 5-chloro-3-hydroxymethyl-indole-2-carboxamide scaffold with apoptotic antiproliferative activity. *Bioorg. Chem.* **2021**, *112*, 104960. [CrossRef] [PubMed]
55. Abbas, S.Y.; Al-Harbi, R.A.; El-Sharief, M.A.S. Synthesis and anticancer activity of thiourea derivatives bearing a benzodioxole moiety with EGFR inhibitory activity, apoptosis assay and molecular docking study. *Eur. J. Med. Chem.* **2020**, *198*, 112363. [CrossRef] [PubMed]
56. Zhang, J.; Yao, T.-W.; Hashizume, R.; Hariono, S.; Barkovich, K.J.; Fan, Q.-W.; Prados, M.; James, C.D.; Weiss, W.A.; Nicolaides, T. Combined BRAF V600E and MEK blockade for BRAF V600E-mutant gliomas. *J. Neurooncol.* **2017**, *131*, 495–505. [CrossRef] [PubMed]
57. Sheldrick, G.M. SHELXT–Integrated space-group and crystal-structure determination. *Acta Crystallogr. Sect. A Found. Adv.* **2015**, *71*, 3–8. [CrossRef]
58. Zhou, G.; Yang, T.; Huang, Z. Structure determination of a low-crystallinity covalent organic framework by three-dimensional electron diffraction. *Commun. Chem.* **2023**, *6*, 116. [CrossRef]
59. Sheldrick, G.M. Crystal structure refinement with SHELXL. *Acta Crystallogr. Sect. C Struct. Chem.* **2015**, *71*, 3–8. [CrossRef]
60. Abou-Zied, H.A.; Youssif, B.G.; Mohamed, M.F.; Hayallah, A.M.; Abdel-Aziz, M. EGFR inhibitors and apoptotic inducers: Design, synthesis, anticancer activity and docking studies of novel xanthine derivatives carrying chalcone moiety as hybrid molecules. *Bioorg. Chem.* **2019**, *89*, 102997. [CrossRef]
61. Youssif, B.G.; Gouda, A.M.; Moustafa, A.H.; Abdelhamid, A.A.; Gomaa, H.A.; Kamal, I.; Marzouk, A.A. Design and synthesis of new triarylimidazole derivatives as dual inhibitors of BRAFV600E/p38α with potential antiproliferative activity. *J. Mol. Struct.* **2021**, *1253*, 132218. [CrossRef]
62. Bollag, G.; Hirth, P.; Tsai, J.; Zhang, J.; Ibrahim, P.N.; Cho, H.; Spevak, W.; Zhang, C.; Zhang, Y.; Habets, G.; et al. Clinical efficacy of a RAF inhibitor needs broad target blockade in BRAF-mutant melanoma. *Nature* **2010**, *467*, 596–599. [CrossRef] [PubMed]
63. Stamos, J.; Sliwkowski, M.X.; Eigenbrot, C. Structure of the Epidermal Growth Factor Receptor Kinase Domain Alone and in Complex with a 4-Anilinoquinazoline Inhibitor. *J. Biol. Chem.* **2002**, *277*, 46265–46272. [CrossRef] [PubMed]
64. Martí-Renom, M.A.; Stuart, A.C.; Fiser, A.; Sánchez, R.; Melo, F.; Šali, A. Comparative Protein Structure Modeling of Genes and Genomes. *Annu. Rev. Biophys. Biomol. Struct.* **2000**, *29*, 291–325. [CrossRef]
65. Muthumanickam, S.; Boomi, P.; Subashkumar, R.; Palanisamy, S.; Sudha, A.; Anand, K.; Balakumar, C.; Saravanan, M.; Poorani, G.; Wang, Y. An Insight of Protein Structure Predictions Using Homology Modeling. In *Computation in Bioinformatics: Multidisciplinary Applications*; John Wiley & Sons, Inc.: Hoboken, NJ, USA; Scrivener Publishing LLC: Beverly, MA, USA, 2021; pp. 265–277.
66. Olsson, M.H.M.; Søndergaard, C.R.; Rostkowski, M.; Jensen, J.H. PROPKA3: Consistent Treatment of Internal and Surface Residues in Empirical pKa Predictions. *J. Chem. Theory Comput.* **2011**, *7*, 525–537. [CrossRef] [PubMed]
67. Halgren, T.A. MMFF VI. MMFF94s option for energy minimization studies. *J. Comput. Chem.* **1999**, *20*, 720–729. [CrossRef]
68. OpenEye Scientific. *SZYBKI 1.9.0.3. 1.9.0.3*; OpenEye Scientific Software: Santa Fe, NM, USA, 2016.

69. Morris, G.M.; Huey, R.; Lindstrom, W.; Sanner, M.F.; Belew, R.K.; Goodsell, D.S.; Olson, A.J. AutoDock4 and Auto-DockTools4: Automated docking with selective receptor flexibility. *J. Comput. Chem.* **2009**, *30*, 2785–2791. [CrossRef]
70. Gasteiger, J.; Marsili, M. Iterative partial equalization of orbital electronegativity—A rapid access to atomic charges. *Tetrahedron* **1980**, *36*, 3219–3228. [CrossRef]
71. Discovery Studio Visualizer (D.S.V.). *Dassault Systèmes BIOVIA. Version 2019*; Dassault Systèmes: San Diego, CA, USA, 2019.